



PAPER • OPEN ACCESS

Enhancing the damping effect of MRF damper using an external magnetic excitation system

To cite this article: Yousif Badri *et al* 2023 *Mater. Res. Express* **10** 095703

View the [article online](#) for updates and enhancements.

You may also like

- [Variable stiffness mechanisms of dual parameters changing magnetorheological fluid devices](#)
Huaxia Deng, Mingxian Wang, Guanghui Han et al.
- [Self-adapting model for variable stiffness magnetorheological dampers](#)
Xinyu Lian, Huaxia Deng, Guanghui Han et al.
- [A novel magnetorheological fluid damper with a heat insulation function](#)
Chengbin Du, Fanang Zeng, Bing Liu et al.

The Breath Biopsy® Guide
Fourth edition

FREE

DOWNLOAD THE FREE E-BOOK

BREATH BIOPSY

OWLSTONE MEDICAL



PAPER

Enhancing the damping effect of MRF damper using an external magnetic excitation system

OPEN ACCESS

RECEIVED

16 June 2023

REVISED

23 August 2023

ACCEPTED FOR PUBLICATION

18 September 2023

PUBLISHED

29 September 2023

Original content from this work may be used under the terms of the [Creative Commons Attribution 4.0 licence](#).

Any further distribution of this work must maintain attribution to the author(s) and the title of the work, journal citation and DOI.

Yousif Badri^{1,*} , Amir Alhams², Sadok Sassi² , Mohammed Hussein³  and Jamil Renno² ¹ Department of Mechanical and Mechatronics Engineering, University of Auckland, Auckland, New Zealand² Department of Mechanical and Industrial Engineering, Qatar University, Doha 2713, Qatar³ Department of Civil and Environmental Engineering, Qatar University, Doha 2713, Qatar

* Author to whom any correspondence should be addressed.

E-mail: ybad223@aucklanduni.ac.nz**Keywords:** semi-active dampers, MRF dampers, magnetic field analysis, magnetic circuit, damping effect, finite element**Abstract**

The magnetic field generated by the damper's magnetic circuit governs the yield stress value of the Magnetorheological Fluid (MRF) damper and hence its damping effect. This paper contributes to the literature on the development of MRF dampers by introducing a new design feature to improve the damper's performance. The presented novel feature tends to amplify the magnetic field value and concentrate its flux within the MR fluid region. The excitation sources consist of 12 coils placed in radial directions surrounding the MRF to focus the energizing magnetic effects. However, the search for efficient solutions is not only focused on generating more energy but also on minimizing its loss. Therefore, a metallic ring was placed around the coils to close the magnetic circuit, guide the flux lines, and avoid any energy dispersion to the surrounding air. As a proof of concept, two materials were tested for the surrounding ring: plastic acrylonitrile butadiene styrene (ABS) and mild steel. The performance of both solutions was assessed experimentally with a Gaussmeter and numerically by using a model developed via COMSOL Multiphysics. Both techniques confirmed the efficiency of the solution based on a steel ring in preventing the flux dispersion into the surrounding air. In addition, an increase of the excitation current from 0 to 5A was found to elevate the magnetic field by 35%, compared with the ABS ring. In the second step, a test rig was designed and built to investigate the damping efficiency of the MRF experimentally. The testing apparatus consisted of a sliding-bearing mechanism connected to a variable speed motor. The damping effect was assessed based on the force and displacement data provided by a linear variable displacement transducer (LVDT) and a force cell. Damping forces were observed at a constant frequency of 0.36 Hz (22 rpm) when the testing system and the attached damper were functioning smoothly away from its resonant frequency. Moreover, the magnetic field excitation current was elevated from 0 A to 5 A with a 1 A step. Again, the metallic ring was found to produce a 112% greater damping coefficient than the case of the plastic ring when the excitation current reached 5A.

1. Introduction

MRF (Magneto-rheological fluid) is an intelligent material for which the rheological behavior can be controlled with the change in the applied magnetic flux (Jolly *et al* 1999). An MRF consists of micro-sized particles that are suspended in a liquid carrier (Metered 2010). Those particles are magnetically polarized and can significantly increase the MRF viscosity (up to 10^3 times) when subjected to a magnetic field (Vékás 2008). However, without a magnetic field, MRF provides similar damping to ordinary oil with moderate viscosity values. The metallic particles in the MRF form a column structure parallel to the flux line. The chain structure arrangement inside the fluid medium develops yield stress known as field-dependent yield stress. The MRFs can be classified depending on the yield stress value and the fluid carrier type (Badri 2022). On the other hand, all devices that use

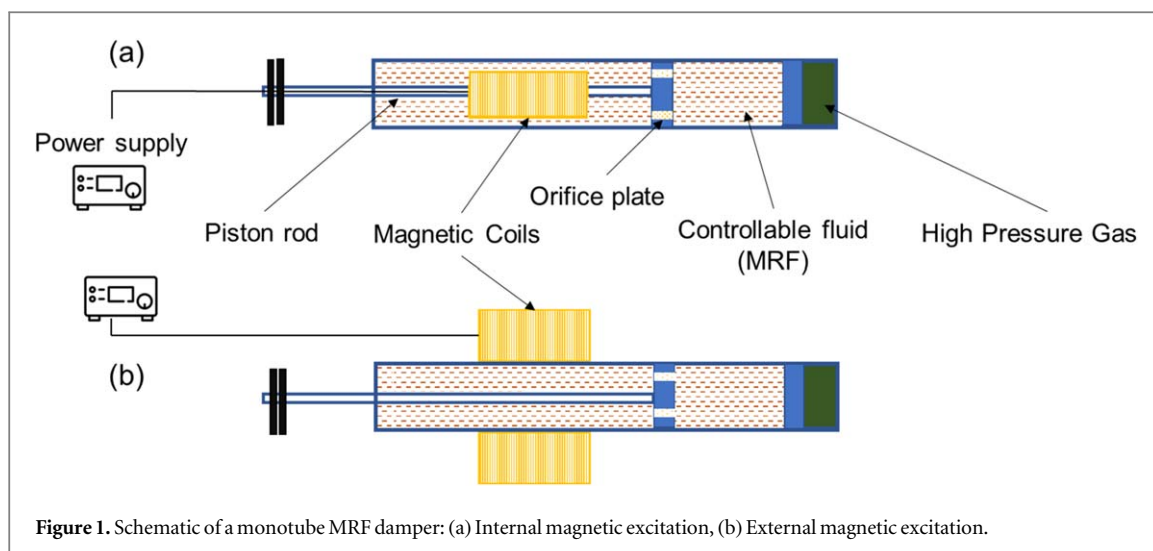


Figure 1. Schematic of a monotube MRF damper: (a) Internal magnetic excitation, (b) External magnetic excitation.

MRFs can be categorized into three operating modes (a) valve mode, (b) direct shear mode, and (c) squeeze mode (De Vicente *et al* 2011). Although all the modes induce a magnetic field perpendicular to the plate's planes, the actuating part changes between the fluid and the plates. For example, in valve mode, the MRF flows because of a pressure gradient between two fixed plates. This mode can be found in applications that include hydraulic controls such as shock absorbers' servo valves. In contrast, the shear mode contains one plate that moves relative to the other plate, which remains stationary. Clutches, brakes, and braking devices use this type of MRF. Lastly, the squeeze mode induces the flow of MRF by applying forces to the two plates in a direction perpendicular to their planes. Because of the small movement of the plates, the squeeze mode is usually adopted in small-amplitude vibration and impact dampers (Zhu *et al* 2012), (Bica *et al* 2013), (Hoyle *et al* 2010). Each of the three operating modes is implemented in different applications where eliminating small/high amplitude/frequency vibrations is needed. One of the first applications that used the valve mode was the suspension element of vehicles known as MRF dampers (Olabi and Grunwald 2007).

The MRF damper is a semi-active vibration countermeasure that supplies different damping values in response to the applied magnetic field. MRF dampers can be controlled to provide a damping effect suitable for various vibration frequencies and amplitudes to deliver maximum working efficiency. The MRF dampers are mainly used in vehicle suspension systems to overcome the limitations of passive Fluid Viscous Dampers (FVD). In vehicle motion, the axle transfers the movement to the vehicle body when the car spring oscillates in response to road imperfections. Therefore, passenger comfort will be disturbed unless the car's suspension system functions efficiently. Efficient damping requires a compromise between safer damping (hard) and comfort damping (soft), which depends both on the damper selection and on the road profile (Soliman and Kaldas 2019). Continuous changes in damping between what is safer for the vehicle and what is required for ride comfort can only be achieved by semi-active damping (Badri 2022).

The MRF damper used in vehicle suspension complies with the conventional shock absorber's fundamental rules and design concepts (Rahman *et al* 2017). Henceforth, the MRF structural configurations discussed in the present work follow the fundamentals of Mono-tube & Twin-tube dampers configurations (Gołdasz and Sapiński 2015). The monotube dampers usually consist of a floating piston that divides the MRF volume into two regions; compression chamber & rebound chamber. The floating piston is attached to a piston rod responsible for transferring the movement of the vibrating structure to the piston (Badri *et al* 2021c). Furthermore, an accumulator containing compressed air and a diaphragm accommodate together the fluid's thermal expansion and prevent MR cavitation. All these internal parts are housed in a single cylindrical tube (Metered 2010), as shown in figure 1(a). In contrast, a twin-tube damper has two concentric cylinder tubes, where the inner one functions similarly to the monotube damper's cylinder. In the absence of compressed air at the Twin-tube, the outer cylinder (reservoir) is designed to accommodate the fluid volume change due to piston rod displacement. By far, the passenger vehicle suspension system is a monotube MRF damper due to its simplicity and few internal components. However, twin-tube dampers are usually used when there is a lack of high-pressure gas packaging. Integrating a magnetic coil into the damper's piston was among the first possible solutions that was used on both types to generate a magnetic field that regulates the MRF flow's resistance inside the damper's cylinder. Depending on the required activation area, the magnetic circuit is built from single coils, or multiple-stage coils wound around the damper's piston and supplied with electric current from an external source (Gołdasz and Sapiński 2015) (figure 1). The induced magnetic flux passes through the MRF region inside the damper and changes the MRF viscosity and hence the shock absorber damping effect. Although this

configuration allows the magnetic flux to pass through the MR fluid gap with minimum magnetic losses (Nguyen and Choi 2009, Gołdasz and Sapiński 2015), its related manufacturing processes are complex and critical. For instance, introducing current wiring to the coils required deep-holing drilling all the way along the piston rod which requires precious machining to ensure straightness and service finish (Sassi *et al* 2018). In addition, the internally excited MRF damper non-flux gap is considered long (Liu *et al* 2022). In order to increase the effective flux-gap the number of coils should be increased. However, such an increase is restricted due to the limited available volume. This fact is another drawback of the internal excitation system. Furthermore, when the coils are powered by an electric current of high intensity, the magnetizing system heat up and has a tendency to radiate heat to the surrounding environment. However, such emitted heat remains trapped inside the damper casing and may change the properties of the MR fluid (Zhu *et al* 2012). Relying on the previous outfalls and seeking simplicity in the machining process, scholars intend to use external magnetic field excitation as a feasible solution rather than internal excitation (Sassi *et al* 2018) (Berasategui *et al* 2014). The magnetic flux generated by the external excitation system has to penetrate the damper cylinder wall to control the MRF behavior. Such a phenomenon may result in magnetic field losses due to the diffuse of flux in the different media next to the system. Those losses are negligible when dealing with the internal excitation system. Furthermore, one of this work's fundamental goals is to minimize the externally magnetic field losses for a better damping effect of the MRF damper.

Regardless of the magnetic circuit location on the damper, the current value, number & volume of coils play a vital role in defining the hard/soft damping behavior of an MRF damper. Therefore, analyzing the damper efficiency usually starts by examining and modeling its magnetic circuit system. Numerous studies have analyzed the magnetic field by solving Ampere's and Maxwell's equations in 2D and 3D (Purandare *et al* 2019), (Biswal and Rao 2016), (Li and Yang 2020), (Hemantha and Arun 2018), (Zheng *et al* 2014). For example, Purandare *et al* analyzed the magnetic field generated in the damper by adopting the finite element (FE) method using COMSOL Multiphysics, and their model was validated by the magnetic circuit theory (Purandare *et al* 2019). A 2D axisymmetric FE model was used to study the MRF, coils, air gap, and damper piston. It was concluded that the magnetic field density increased linearly as the current increased. Moreover, the material's magnetic permeability was found to play an essential role in the intensity of the magnetic flux across the damper. In addition to the current and the material's permeability, other factors can affect the magnetic field's intensity and, thus, the yield stress of the MRF. For example, the diameter of the core, the number of coil stages, the arrangement of the magnetic poles, and the damping channel's width affect the magnetic field density. Consequently, (Ju 2019) conducted a 2D and 3D magnetic circuit optimization study to investigate the effects of these parameters on the magnetic field intensity (Ju 2019).

All experimental studies on MRF dampers were conducted to obtain the model's parameters statistically or to validate the models of the MRF dampers (Warke *et al* 2022). For example, Guan *et al* (2019) designed a test bench to investigate their twin-tube shock absorber that consisted of a motor, a load rack, a static frame, and a 25-mm radius crank (Guan *et al* 2019). The crank transformed the motor's rotational movement into a linear reciprocating motion. The loading rack was connected to the crank through a linkage and then attached to the damper. Meanwhile, a force cell was located at the bottom of the bench to record the damping force via a data acquisition system. Their objective was to obtain force-velocity and force-displacement curves, then compare them with the numerical model results. They found that the damping force decreased at the end of the compression stroke. However, the testing mechanism was governed by the crank slider (scotch yoke). In addition to the crank slider movement, Iglesias *et al* (2014) used a mechanical exciter in their MRF damper's experimental setup (Iglesias *et al* 2014). The mechanical exciter consists of a variable-speed motor with a cam system. It provides the necessary dynamic load up to 500 N with 0.1–3 Hz. A Linear Variable Displacement Transducer (LVDT) sensor and a force cell were mounted on the damper to measure the damper's performance. The required excitation current was provided by a DC power supply that was connected to the MRF's electromagnetic system coils. Subsequently, all the sensors were connected to a data acquisition device that recorded the displacement–force data.

On the other hand, some scholars used specially made devices known as damper test systems (Iglesias *et al* 2014). In their investigations, Iglesias *et al* used an MTS-835 damper testing system that can reach up to 15 kN with a maximum stroke length of 100 mm (MTS Manual 2012). Moreover, their testing machine could provide a wide range of excitation waveforms. The variety of excitation forms gave advantages over the motor-based experimental setup. The MRF damper study was carried out by a particular excitation where harmonic oscillations were imposed with increasing frequencies (frequency sweep). In addition, another test was conducted by increasing the load amplitudes for a fixed frequency (amplitude sweep). In all the tests, the excitation current values were raised by a constant step of 1 A, from 1 A to 6 A. The damper system helped them find the damping force's behavior for a wide range of frequencies and amplitudes. However, the performance of any MRF damper investigated previously in the literature depended on optimizing numerous parameters (type of MRF, piston stroke, valves dimensions, piston diameter, number of coils, direction of the coils, diameter of

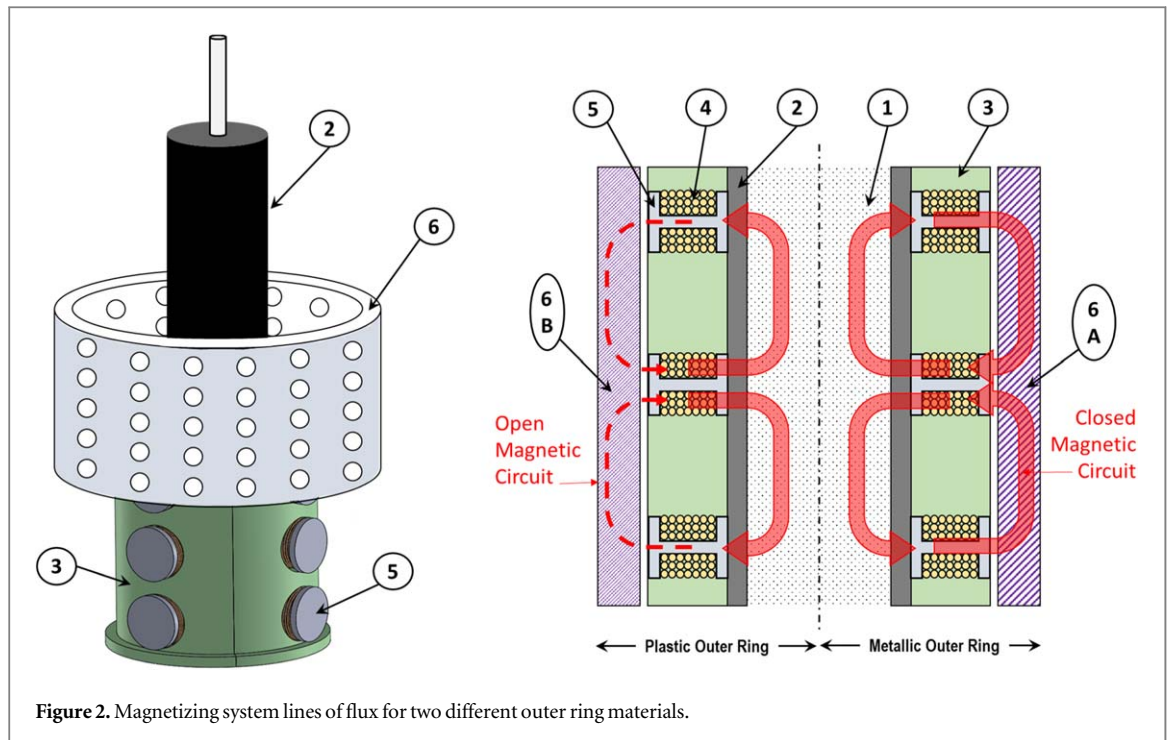


Figure 2. Magnetizing system lines of flux for two different outer ring materials.

the wires, current intensity, etc) (Nguyen *et al* 2007, Nguyen *et al* 2008, , Nguyen and Choi 2009, Badri *et al* 2021a, 2021b).

In the present study, a modern design feature is introduced for the first time, which enables one to change the magnetic field's intensity without changing the coil's turns, the current value, or even the direction of the coils. This feature involves attaching a ring that envelops the magnetic excitation set externally. This practical novel design feature will enhance the performance of externally excited MRF dampers with no further requirements of expensive and complicated manufacturing processes. The magnetic and damping effect corresponding to the attachment of the ring will be investigated numerically and experimentally in the following sections.

2. Design of the MRF damper

The MRF damper investigated in this study represents an improved version of the damper initially developed by (Sassi *et al* 2018) which was slightly modified to incorporate an industrial magnetological fluid (1) MRF-132DG (Lord Tech 2019). The initial design consisted of a standard fluid damper (2) was modified by cutting the damper's tip and substituting it with a threaded cap. Hence, emptying the damper from its original oil and filling it with MRF-132DG become easier and do not require sealing. As depicted in figure 2, the magnetizing system consisted of a coils' holder (3) made of two identical plastic parts obtained by 3D printing. This assembly surrounds the cylinder along a distance of about 10 cm and can accommodate 12 coils placed in four rows of three coils each. Each of the coils consist of 170 turns of 18AWG copper wire 1 mm in diameter (4) looped around a metallic core (5) with a particular shape that precisely touches the outer surface of the damper.

As the coils' holder (3) was made of two halves, an external ring (6) was needed to keep them locked to each other and ensure good contact between all metallic parts (from the cores up to the damper body). However, as the initial external ring was made from plastic (6B), its low magnetic permeability prevents the flux lines from flowing easily and leaves the magnetic system in a quasi-open state. Therefore, using a new metallic ring (6A) was highly recommended. The entire excitation system and the two surrounding rings of the parametric study addressed in this paper are displayed in figure 3.

3. Comsol magnetic field analysis

Partial differential equations governing the interaction of the magnetic field with the MRF are challenging to develop and solve. Thus, the FE method provided an attractive alternative approach to modeling the systems. In this work, we used the AC/DC module of COMSOL Multiphysics to solve this problem numerically. A magnetic field (MF) interface was selected to simulate the excitation system of the MRF damper. This type of interface is used when the magnetic field and the induced current's distributions in and around coils, conductors, and

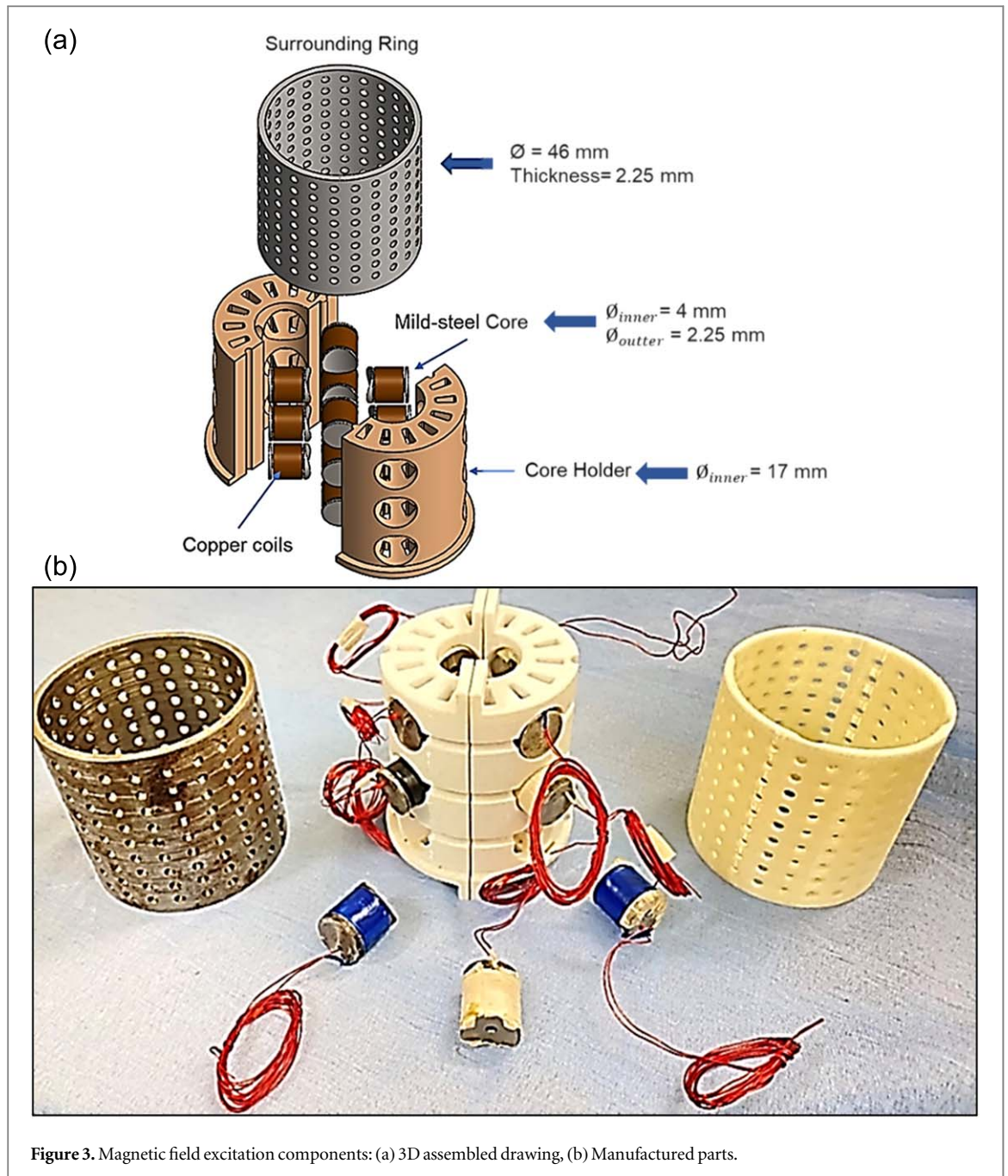


Figure 3. Magnetic field excitation components: (a) 3D assembled drawing, (b) Manufactured parts.

magnets are calculated and analyzed (COMSOL Multiphysics 2018). Moreover, this physical interface provides material models that are typically used in magnetic field applications, such as copper, soft iron, and plastic insulators. The following section will describe the phases of conducting the magnetic field analysis of the MRF core excitation system. A 3D SolidWorks model was developed for the entire excitation system (figure 4). The magnetic field excitation system consists of three main parts: cores, the core holder, and the surrounding ring, as shown in figure 5. In addition to simulations, 3D drawings were used for manufacturing the MRF damper excitation system. The MRF excitation system developed by (Sassi *et al* 2018) presented the starting point for further work and improvements in this study. In other words, the same number of cores and core holder dimensions as in the previous study (Sassi *et al* 2018) were considered in the present investigation. However, the core design was enhanced to involve more coil turns and allow for more interaction between the core and the surrounding ring. In addition, the upper ventilation openings of the core holder were increased in number and dimensions to improve cooling by natural convection. The SolidWorks 3D drawing created four main domains: the holder, the ring, the cores, and the coils. The coils were modeled as a solid cylinder surrounding the core body's middle part, as shown in figure 5.

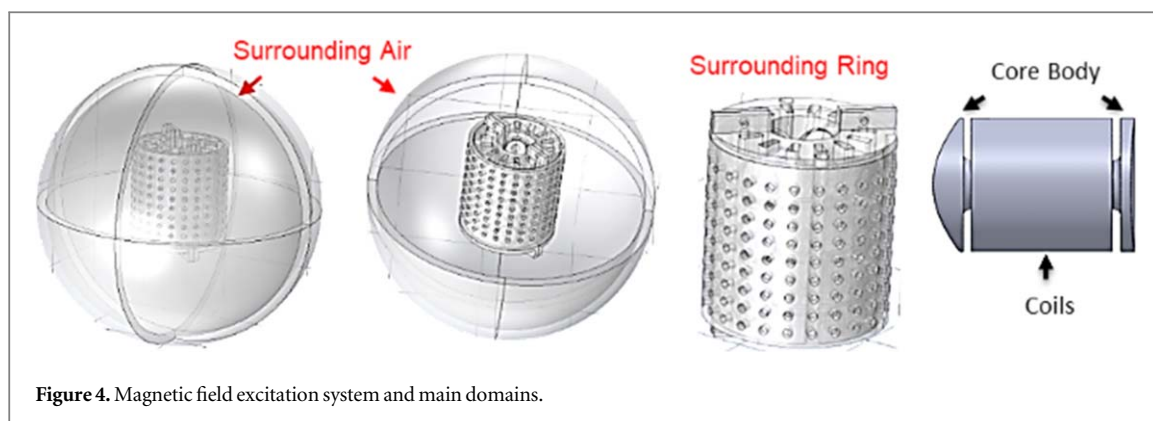


Figure 4. Magnetic field excitation system and main domains.

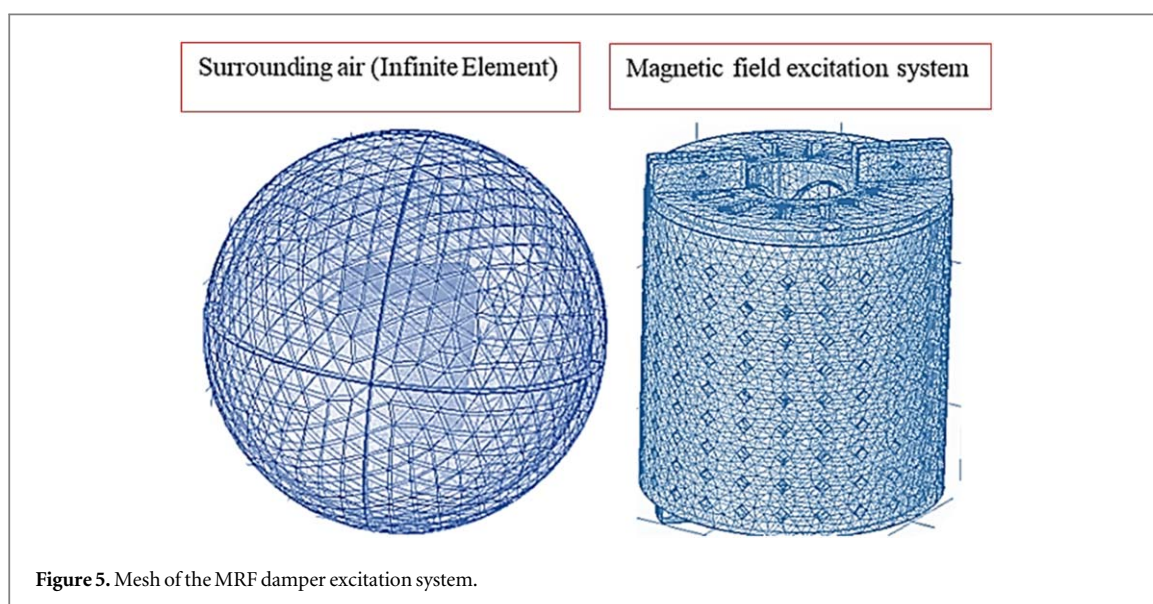


Figure 5. Mesh of the MRF damper excitation system.

3.1. Meshing

Meshing was done by using the built-in physical controlled meshing feature of COMSOL. Usually, with an automatic mesh, tetrahedral elements are created with a predefined size. With the physics-controlled mesh setting and finer mesh size, 327,043 tetrahedral elements were needed to simulate the entire domain, with a 5.419×10^{-8} element volume ratio and a mesh volume of 0.01405 m^3 . To ensure the solution process generated an acceptable level of accuracy, a sensitivity analysis was needed to ensure that the solution was independent of the mesh size and the number of elements. In addition, the mesh's statistical quality parameters were also used as indicators of the solution's accuracy. For example, the skewness parameter was defined as the angular measure of the quality of elements. It illustrates how ideal a cell or a face is (COMSOL Multiphysics® | COMSOL Blog). In the model's actual meshing, the skewness quality value was found to be 0.615. As this was larger than the minimum value of 0.01, this quality indicator ensured an excellent mesh quality (COMSOL Multiphysics® | COMSOL Blog).

3.2. The electromagnetic excitation system's boundary conditions

Firstly, for the sake of calculation, an infinite element was needed to surround the system under investigation. Therefore, a spherical domain of 0.1 m in diameter simulated the air volume surrounding the excitation system. Secondly, the materials were selected for each domain (part) with the built-in properties of the COMSOL material library, as illustrated in table 1.

The coils were modeled as multi-turn circular copper wires. The number of turns was set to 180, which replicated the real-case design of the coils. The electric current values were increased from 1 A to 5 A with an increment of 1 A. An MF study, including Ampere's law, magnetic insulation, and initial value equations, was applied to the stationary study. The MF analysis was conducted five times (1–5 A) for the two surrounding rings made from different materials (mild steel and ABS). The computational time for each case was approximately 30 min.

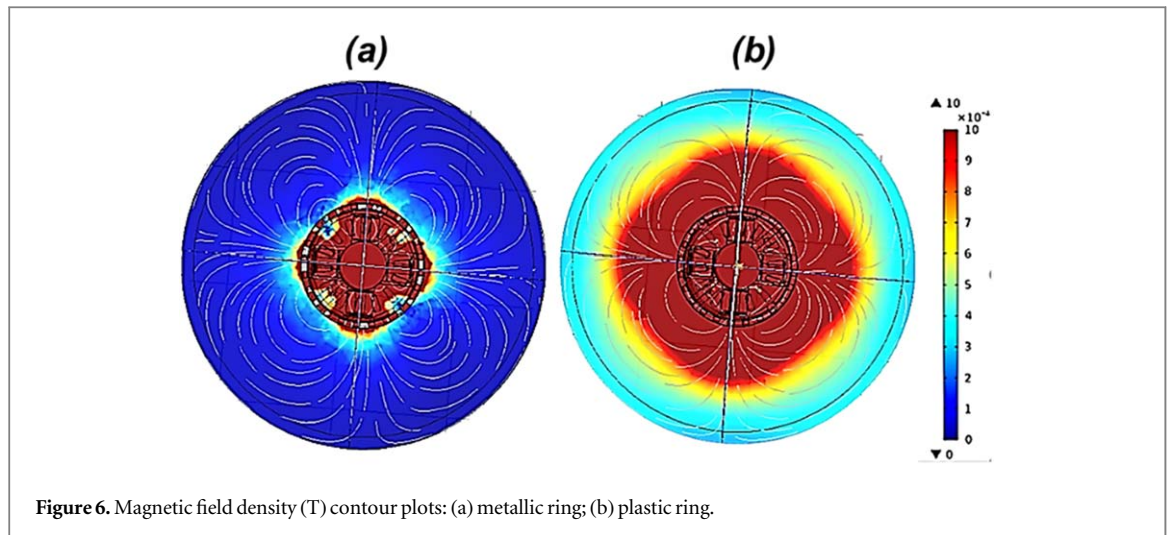


Figure 6. Magnetic field density (T) contour plots: (a) metallic ring; (b) plastic ring.

Table 1. Materials' electromagnetic properties.

Domain	Materials	Relative Permeability ($\frac{\mu}{\mu_0}$)	Relative Permittivity ($\frac{\epsilon}{\epsilon_0}$)	Electrical Conductivity (Siemens per meter-S/m)
Infinite Element	Air	1	1	0
Core	Mild Steel	6000	0.001	1.12×10^{-7}
Coils	Copper	1	1	5.87×10^{-7}
Plastic-Holder	ABS	1	1	7.05
Surrounding-Ring	ABS	1	1	7.05
	Mild Steel	6000	0.001	1.12×10^{-7}

3.3. Numerical model results of COMSOL

The main aim of the COMSOL magnetic simulation was to define the differences between the two materials used for the surrounding ring. The main properties affecting the magnetic field density were the permeability, permittivity, and electrical conductivity of the two materials (plastic and mild steel). Figure 6 clearly shows the differences in magnetic field density between the two cases.

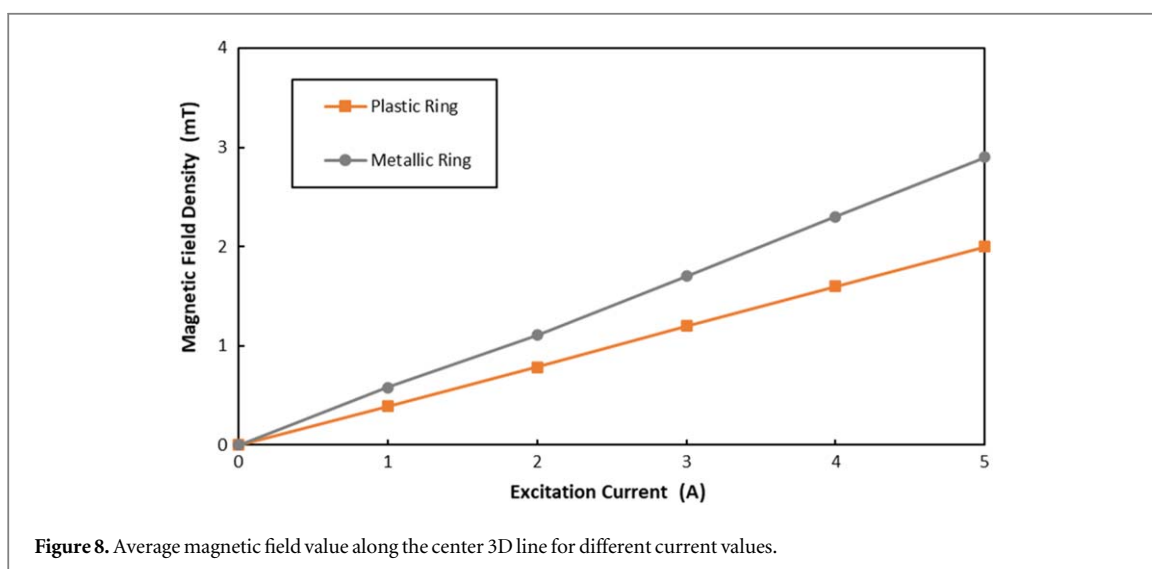
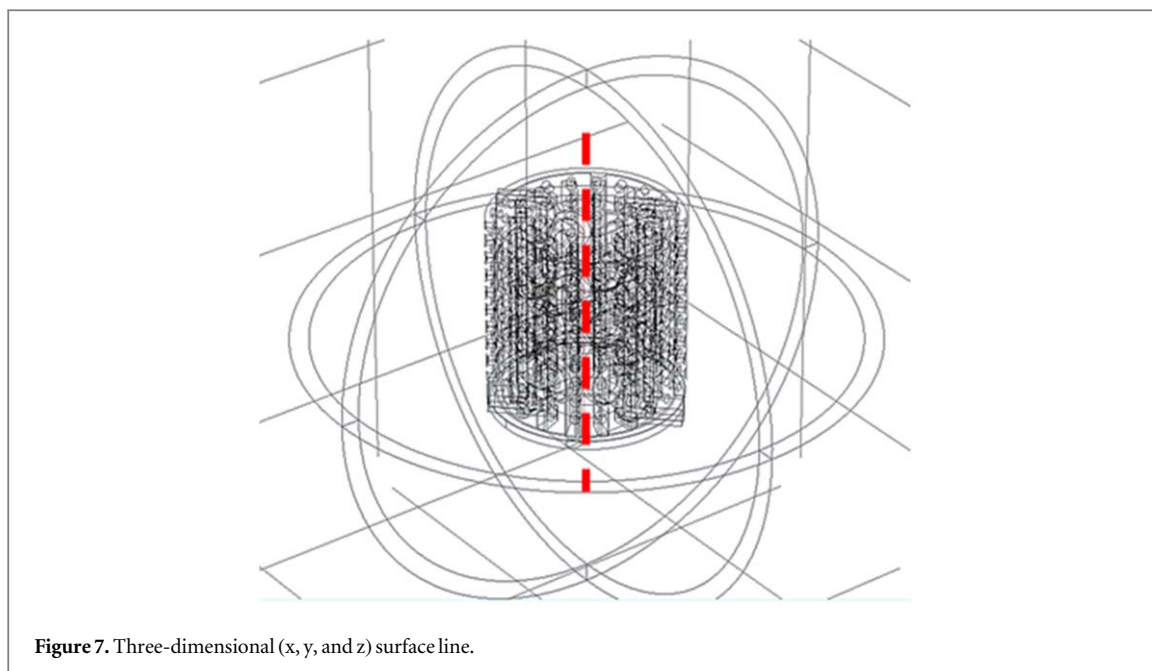
In the previous contour plots, one can see that when the surrounding ring is made of ABS, there is massive magnetic field radiation to the adjacent volume, creating a non-negligible loss of energy. On the other hand, when the ring is made of steel, the lines of flux are smoothly guided inside the ring, the magnetic circuit is therefore fully closed, and radiation to the outside is greatly minimized.

To quantify the effect of the ring material on the magnetic field density inside the MRF chamber, a 'Section Cut' was created in a 3D coordinate ($x-y-z$) system, displayed in figure 7. In COMSOL, a straight line passing through the volume of interest allowed the magnetic field density to be read at those specific locations.

Because the readings along the 3D line were variable, the average value was computed and plotted (figure 8). When the excitation current increased, the magnetic field density grew linearly for both materials but at different rates. For the steel ring, the magnetic effect was always more pronounced than that created with the plastic ring. This difference was around +24% for a current of 1 A and +44% when the current was 5A.

A comparison with experimental results is highly needed to validate the MF numerical model. Therefore, a gaussmeter was used to measure the field density value at a reference line located at the center of the excitation system, as shown in figure 9. The 'FW Bell Gauss/Tesla' meter used in validating the model results has a transverse probe where the sensitive area is located at its tip. The probe was placed manually at the red cross center point illustrated in figure 9.

The measurements taken for the settings previously described were recorded in milli-Tesla (mT) for both ring materials and plotted, in figure 10, against the numerical results from COMSOL. One can see that the numerical model results are very close to the experimental ones, with a maximum error of 12%. The discrepancy between both sets of results is probably related to two significant reasons. First, the inconsistency in the permeability, permittivity, and electric conductivity values of all model elements and domains has made the numerical model generate results that do not match experimental ones and are always higher (figure 10). Second, the numerical results displayed in figure 10 are obtained from different approaches. While numerical model results were based on averaging the magnetic field values numerical values obtained along the 3D center



line (figures 7 and 9), the experimental readings provided by the tip of the Gaussmeter probe were sensed from a narrow area.

4. Experimental testing of the MRF damper

The experimental setup developed in this (shown in figure 11) consisted of two main parts (the frame, and the motor and scotch yoke). Extra components (sliding bearings) ensured proper sliding of the moving parts. The test rig frame comprised two parallel plates fixed on four steel bars. Long neck flanges were placed at the end of each bar to ensure the system's stability. A scotch yoke mechanism was attached to the motor to transform the rotational motion into a linear oscillating motion. The MRF damper was attached to this setup by connecting its moving rod to the scotch yoke moving plate and maintaining the damper's other end attached to the upper fixed plate through a force cell.

Two sensors were used and installed on the test rig to quantify the dynamic behavior of the damper. First, a linear variable differential transducer (LVDT-100M from Loadstar Sensors) with 100-mm stroke reading capacity was nestled between the body of the damper and the scotch yoke plate and recorded the linear displacements with an error of 0.02% on the full scale. Secondly, an S-Beam load cell sensor (RAS1-100S-S from

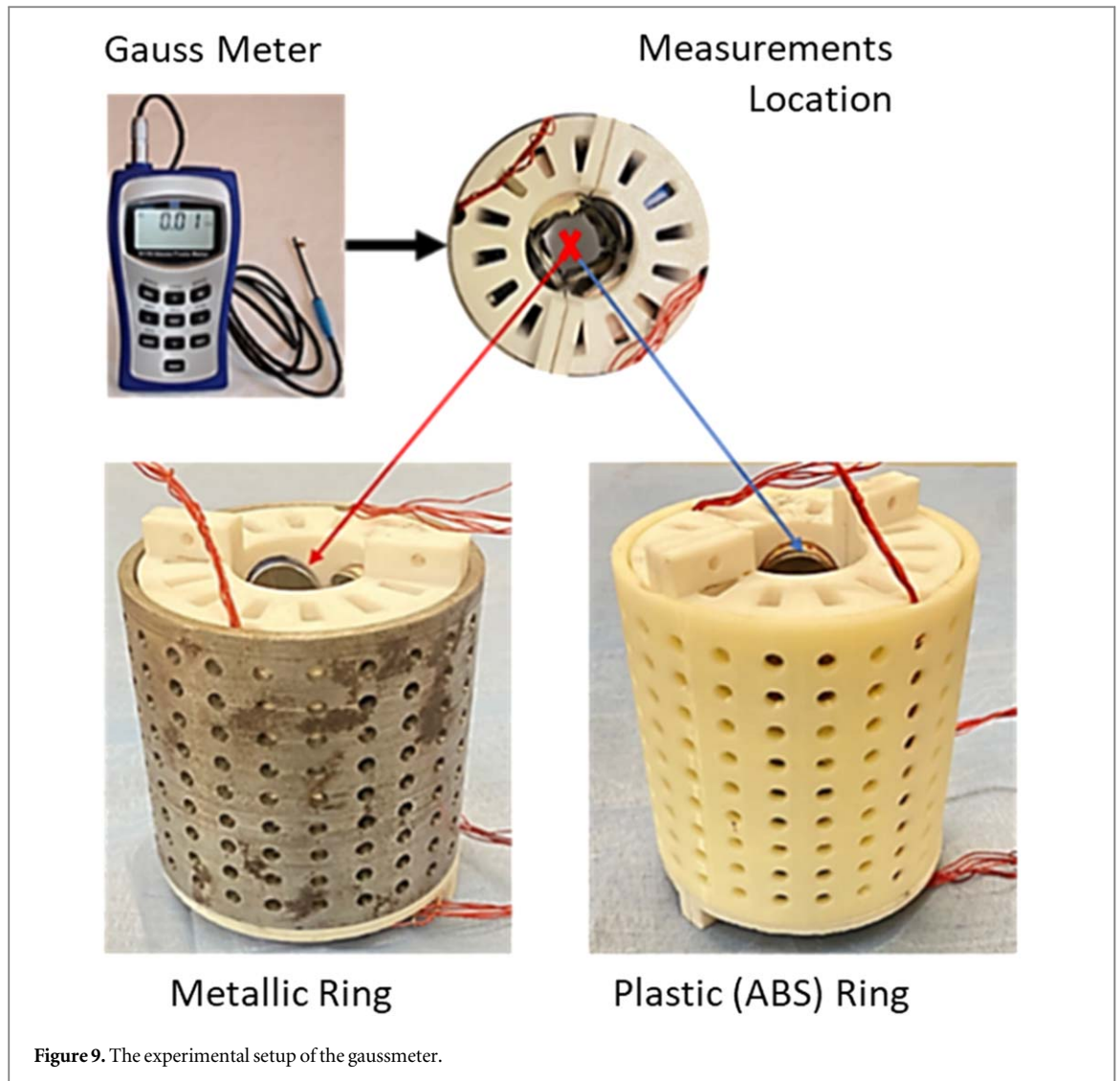


Figure 9. The experimental setup of the gaussmeter.

Loadstar Sensors) was placed in series with the damper to record the damping force in response to the motor's movement. It can sense up to 444.8 N with an error of 0.01% on the full load.

A variable-frequency drive (VFD) (Schneider, 3 kW, ATV312HU30N4) maintained the motor's rotational speed at a fixed value (Error: ± 0.1 Hz) of 22 RPM (0.115 m s^{-1}) to ensure constant experimental robustness conditions during all tests. All readings were acquired by a Loadstar Acquisition system, which consisted of two resistive interfaces and SensorVUE software at a reading rate of 0.1 s. All the cores were joined in parallel and connected to a DC power supply through two connecting points, providing the optimized magnetic pole arrangement reported in (Sassi *et al* 2018). Five different values of excitation current were used (1,2,3,4, and 5A).

5. Results and discussion

Once the test rig was completely mounted and tuned, two sets of experiments were conducted on the MRF damper with the metallic and plastic rings. In each test, the MRF damper was subjected to a harmonic load from the sliding motor setup at a constant frequency of 0.36 Hz, and the current applied to the coils was kept at a constant value. In addition to the testing apparatus' robustness running conditions, the fixed frequency of 0.36 Hz was selected seeking for velocity range that emphasize the possibility of obtaining equivelant linear damping constant. Figure 12 portrays an example of a force-displacement loop obtained from the displacement and force readings for the case of a 1-A excitation current. The smoothness of the circular patterns in the force-displacement space depended on the motion quality (pure harmonic or not) provided by the experimental setup, and on the flow of the fluid inside the damper (Badri *et al* 2021a). In our case, none of the previous conditions were observed, especially for the force results; therefore, a filtering tool (summation of sine curve fitting by MATLAB) needed to be applied. Figure 12 an example of the experimental data of the damping forces

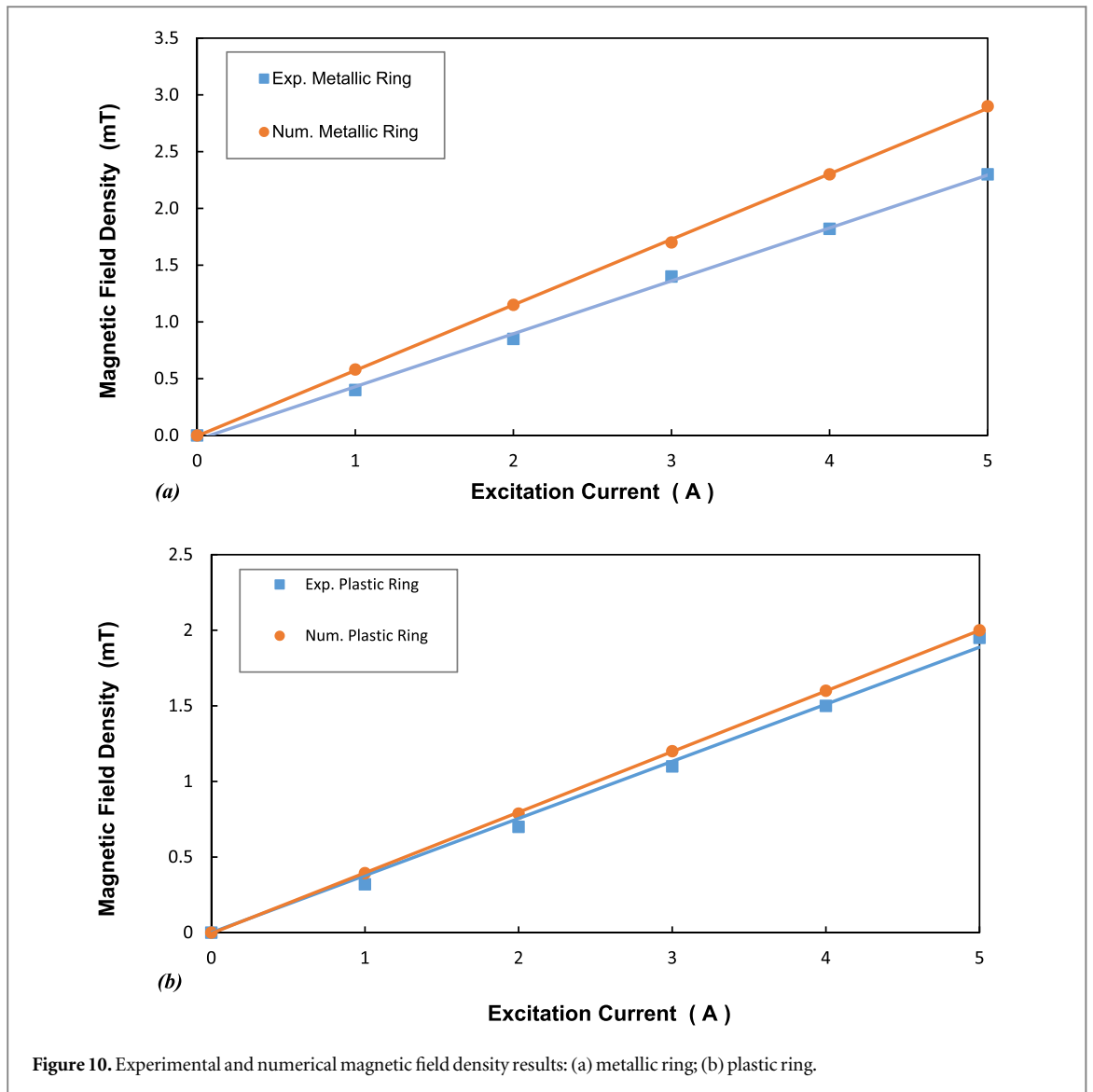


Figure 10. Experimental and numerical magnetic field density results: (a) metallic ring; (b) plastic ring.

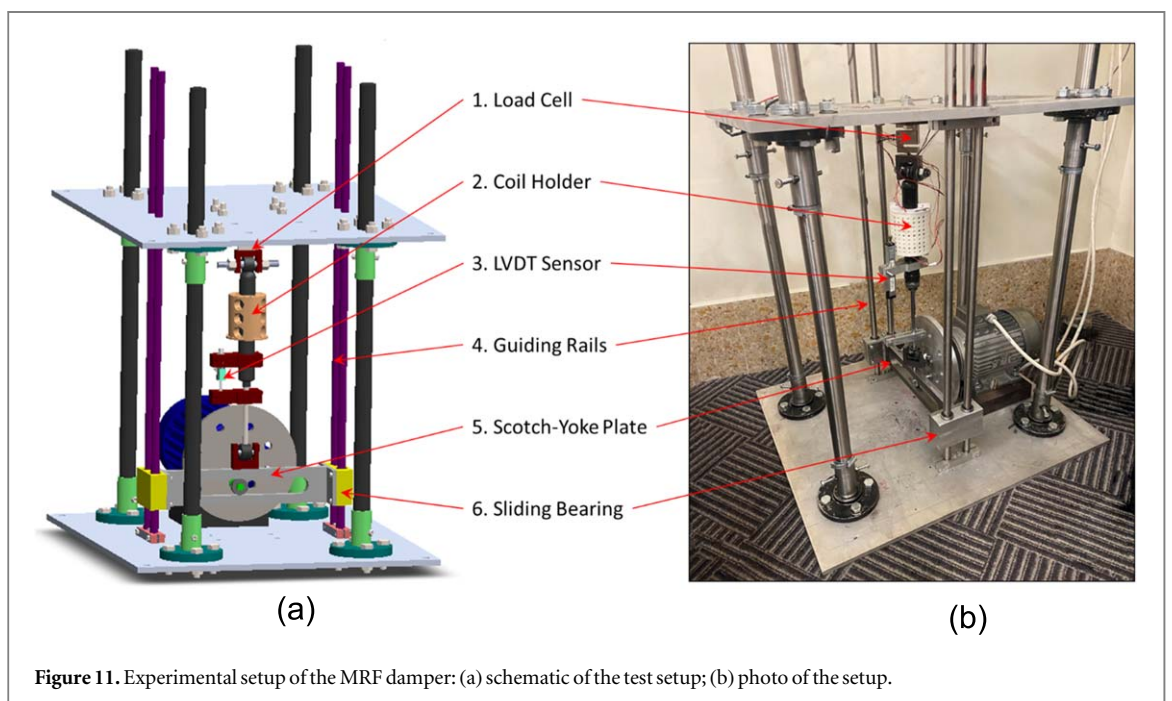


Figure 11. Experimental setup of the MRF damper: (a) schematic of the test setup; (b) photo of the setup.

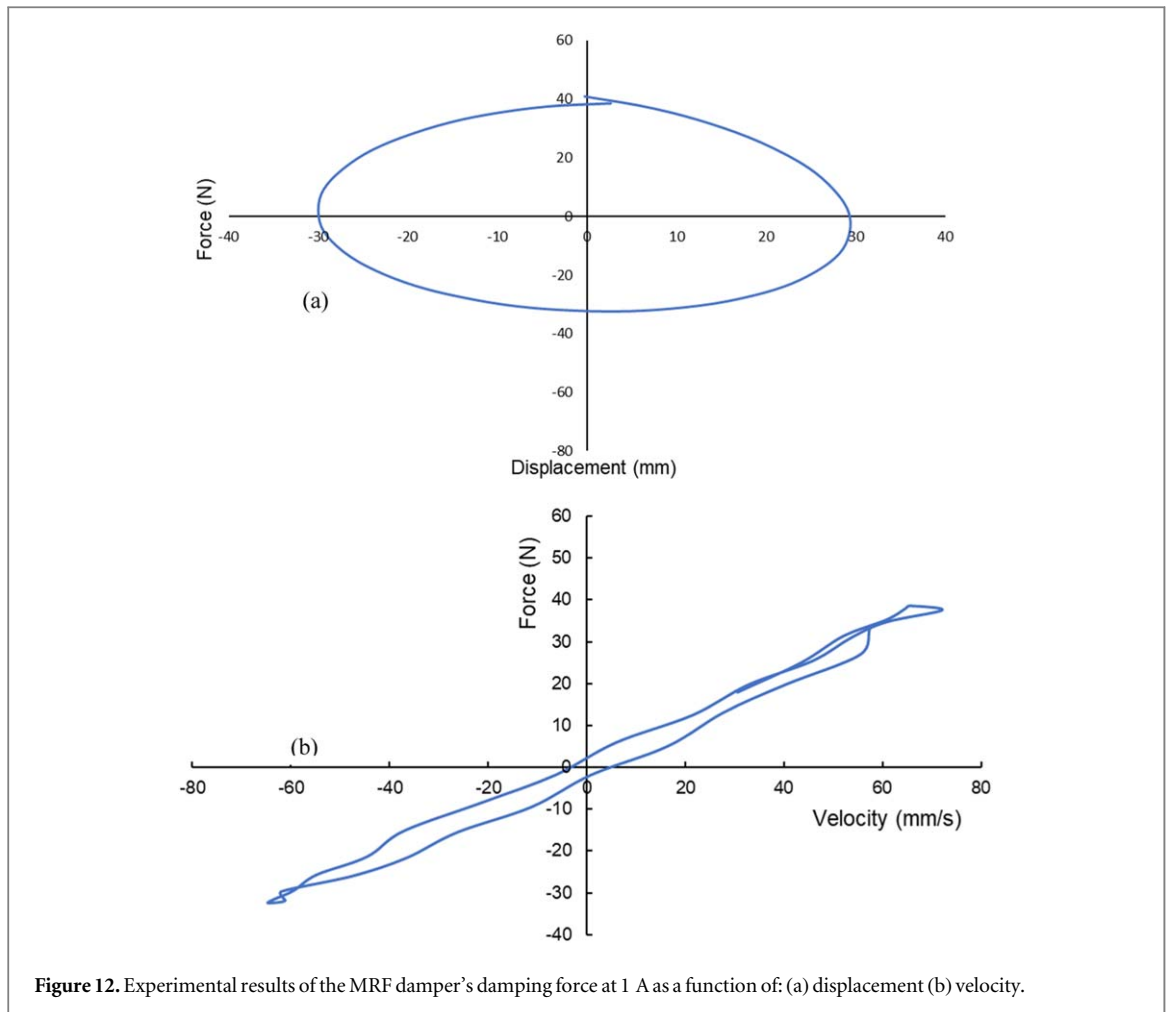


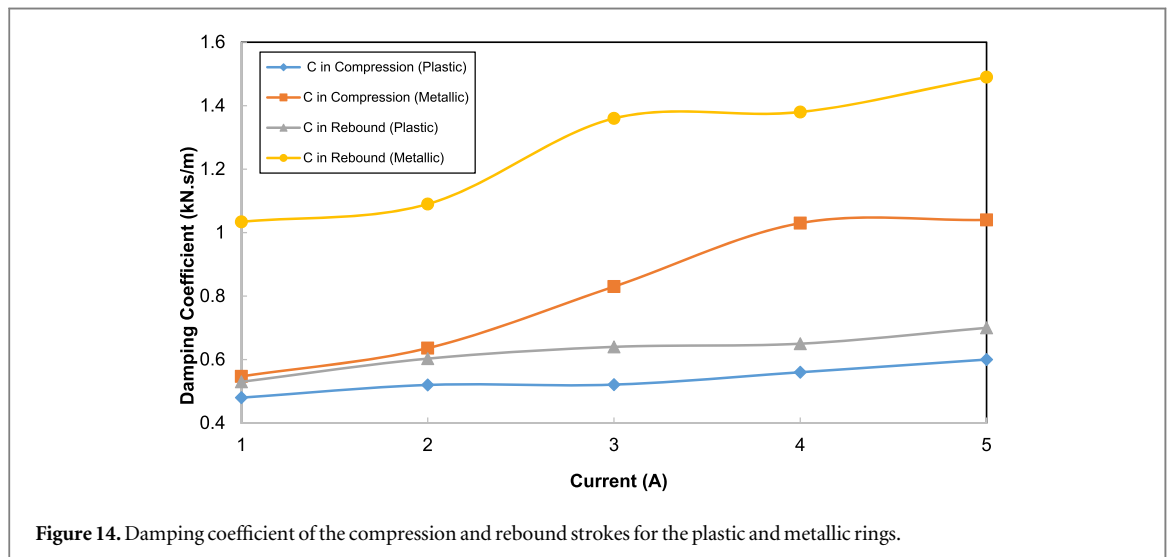
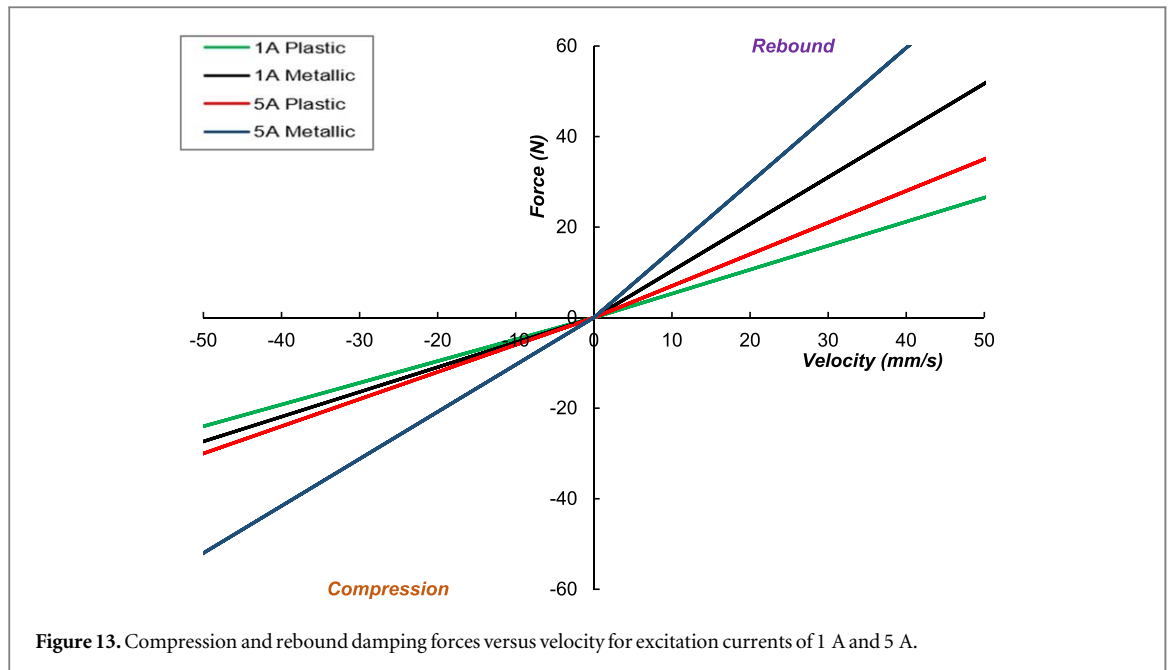
Figure 12. Experimental results of the MRF damper's damping force at 1 A as a function of: (a) displacement (b) velocity.

at 1A as a function of displacement and velocity. One can easily see the hysteresis behavior in the force-velocity graph (figure 12(b)).

To assess the effect of the excitation current flowing inside the coils on the damper's overall performance, the damping coefficient values must be obtained for the rebound and compression strokes. For FVD undergoing harmonic motion, when applying moderate values of forces and velocities (frequencies), the damper's displacement u_t at a time interval t , over the maximum displacement u_0 is equal to one, according to the analytical generalized non-linear FVD model in (Lin and Chopra 2002). In this condition, the relationship of force versus velocity could be reasonably considered linear (Lin and Chopra 2002). In addition, uniform low magnetic field values limit the non-linear increase of the shear yield strength, hence decreasing the Force-Velocity non-linear hysteresis behavior (De-Kui *et al* 2018). As the experiment considered those conditions that decrease the non-linear effect, the MRF damper was assessed based on Constant C values. Furthermore, linear interpolations were calculated for the force-velocity results in the rebound and compression strokes. The force-velocity data at each stroke were linearized separately using the Matlab curve fitting toolbox, to obtain the two constant values of damping constants (C) at compression and extension. As reported in the literature [20, 23–25], the damping forces of the rebound stroke are more significant than those obtained for the compression strokes. The results displayed in figure 13 also show an increase in the damping forces (rebound and compression) as the excitation current value increased.

To summarize the numerical and experimental developments previously revealed, the damping coefficients of the MRF damper equipped with plastic and metallic rings were obtained for the extension and compression strokes. The viscous damping parameters were obtained by first-order polynomial fitting and then plotted as a function of the supplied current, as shown in figure 14.

From the results displayed in figure 14, one can see that when the current increases to 5A, the damping effect is linear and remains minor in the case of a surrounding ring made of plastic (a $\sim 25\%$ increase in compression and a 32% increase in rebound). However, when the ring is made of steel, the variation in the damping is nonlinear and more noticeable (a 96% increase in compression and a 49% increase in rebound).



6. Conclusion

This paper presented the design, manufacture, and testing of an MRF damper equipped with a magnetic excitation system inserted inside an outer ring made from two different materials: ABS plastic and mild steel. The study's main objective was to quantify the effect of the surrounding ring's material on the generated magnetic fields and its corresponding damping behavior. The magnetic field analysis and the experimental damping effect of the MRF damper for the two developed rings led to the following conclusions.

- Surrounding the excitation system of cores with a ring made from mild steel will concentrate the magnetic density value at the volume of interest (inside the damper's main chamber filled with MRF). In contrast, plastic (ABS) will dissipate the magnetic field within a large volume around the interest zone.
- Metallic (mild steel) rings amplify the magnetic field density value by almost 35% compared with the magnetic density of plastic (ABS) rings. The FE-Model magnetic field values are always higher than the experimental ones, and the maximum divergence reached 12% for the case of the metallic ring. The differences in results are much related to the model boundary condition values and the different sensing techniques adopted for both the numerical and experimental approaches.

- For both the plastic (ABS) and the metallic rings, the damping coefficients in the rebound and compression strokes increased by 7% to 13% as the current increased by 1A across the excitation current range of 1–5A.
- The damping forces measured when the metallic ring was attached to the magnetic circuit were much higher than those obtained with the plastic ring. Moreover, across the excitation current range of 1–5A, the compression damping coefficients increased by 14%–73.3% for the plastic ring. On the rebound side, the effect of the metallic ring was 80% to 112% greater than that of the plastic ring.

Acknowledgments

Financial support for this research was graciously provided by Qatar National Research Fund (a member of Qatar Foundation) via the National Priorities Research Project under Grant No. NPRP-11S-1220-170112.

Data availability statement

All data that support the findings of this study are included within the article (and any supplementary files).


Declaration of conflicting interests

The author(s) declared no potential conflicts of interest with respect to the research, authorship, and/or publication of this article.

ORCID iDs

Yousif Badri  <https://orcid.org/0000-0001-6661-410X>

Sadok Sassi  <https://orcid.org/0000-0002-1104-8099>

Mohammed Hussein  <https://orcid.org/0000-0003-2594-5804>

Jamil Renno  <https://orcid.org/0000-0002-1081-9912>

References

- Badri Y 2022 An experimental and numerical investigation of the combination of different damper types for improved control of vibration *Qatar University*
- Badri Y, Sassi S, Hussein M and Renno J 2021 Experimental and numerical investigation of damping in a hybrid automotive damper combining viscous and multiple-impact mechanisms *J. Vib. Control* **36**76–87
- Badri Y, Syam T, Sassi S, Hussein M, Renno J and Ghani S 2021 Numerical study on the damping characteristics of a shock absorber valve utilizing different velocities through CFD analysis *8th International Conference on Computational Methods in Structural Dynamics and Earthquake Engineering* pp 4353–62
- Badri Y, Syam T, Sassi S, Hussein M, Renno J and Ghani S 2021 Investigating the characteristics of a magneto-rheological fluid damper through CFD modeling *Mater. Res. Express* **8** 055701
- Berasategui J, Elejabarrieta M J and Bou-Ali M M 2014 Characterization analysis of a MR damper *Smart Materials and Structures* **23** 045025
- Bica I, Liu Y D and Choi H J 2013 Physical characteristics of magneto-rheological suspensions and their applications *J. Ind. Eng. Chem.* **19** 394–406
- Biswal T and Rao L B 2016 Analysis of the magnetic field for MR damper working in shear mode *Int. J. Struct. Eng.* **7** 48–62
- COMSOL Multiphysics® | COMSOL Blog 2022 Available at: <https://comsol.com/blogs/how-to-inspect-your-mesh-in-comsol-multiphysics/>
- COMSOL Multiphysics 2018 AC/DC Module User's Guide
- De-Kui X et al 2018 Characteristics, optimal design, and performance analyses of MRF damper *Shock and Vibration* **2018** 17
- De Vicente J, Klingenberg D J and Hidalgo-Alvarez R 2011 Magnetorheological fluids: a review *Soft Matter* **7** 3701–10
- Gołdasz J and Sapiński B 2015 *Insight into Magnetorheological Shock Absorbers* (Switzerland: Springer International Publishing) (<https://doi.org/10.1007/978-3-319-13233-4>)
- Guan D, Jing X, Shen H, Jing L and Gong J 2019 Test and simulation the failure characteristics of twin tube shock absorber *Mech. Syst. Signal Process.* **122** 707–19
- Hemantha T M G and Arun K 2018 An approach for characterizing twin-tube shear-mode magneto-rheological damper through coupled FE and CFD analysis *J. Brazilian Soc. Mech. Sci. Eng.* **40** 1–14
- Hoyle, Arzanpour S and Shen Y 2010 A novel magneto-rheological damper based parallel planar manipulator design *Smart Mater. Struct.* **19** 055028
- Iglesias G R, Ahualli S, Echavarrri Otero J, Fernández Ruiz-Morón L and Durán J D G 2014 Theoretical and experimental evaluation of the flow behavior of a magnetorheological damper using an extremely bimodal magnetic fluid *Smart Mater. Struct.* **23** 11
- Jolly M R, Bender J W and Carlson J D 1999 Properties and applications of commercial magnetorheological fluids *J. Intell. Mater. Syst. Struct.* **10** 5–13
- Ju B 2019 The simulation and optimization of the magnetic circuit for magnetorheological damper *Int. J. Magn. Electromagn.* **5** 1–9
- Li G and Yang Z-B 2020 Modelling and analysis of a magneto-rheological damper with nonmagnetized passages in piston and minor losses *Shock and Vibration.* **2020** 12

- Lin W-H and Chopra A K 2002 Earthquake response of elastic SDF systems with non-linear fluid viscous dampers *Earthquake Engng Struct. Dyn.* **31** 1623–42
- Liu L, Xu Y, Zhou F, Hu G and Yu L 2022 Performance Analysis of Magnetorheological Damper with Folded Resistance Gaps and Bending Magnetic Circuit *Actuators* **11** 165
- LORD TECHNICAL DATA 2019 MRF-132DG Magneto-Rheological Fluid *USLORD Corporation*
- Metered H A 2010 Modelling and control of magneto-rheological dampers for vehicle suspension systems *Ph.D. Thesis* University of Manchester
- Nguyen Q H and Choi S B 2009 Optimal design of a vehicle magnetorheological damper considering the damping force and dynamic range *Smart Mater. Struct.* **18** 015013
- Nguyen Q H, Choi S B and Wereley N M 2008 Optimal design of magnetorheological valves via a finite element method considering control energy and a time constant *Smart Mater. Struct.* **17** 025024
- Nguyen Q H, Han Y M, Choi S B and Wereley N M 2007 Geometry optimization of MR valves constrained in a specific volume using the finite element method *Smart Mater. Struct.* **16** 2242–52
- Olabi G and Grunwald A 2007 Design and application of magnetorheological fluid *Materials and Design* **28** 2658–64
- Purandare S, Zambare H and Razban A 2019 Analysis of magnetic flux in magneto-rheological damper *J. Phys. Commun.* **3** 075012
- Rahman M et al 2017 A review of advances in magnetorheological dampers: their design optimization and applications *J. Zhejiang Univ. Science A* **18** 991–1010
- Sassi S, Sassi A, Cherif K and Tarlochan F 2018 Magneto-rheological damper with external excitation for more efficient control of vehicles' dynamics *J. Intell. Mater. Syst. Struct.* **29** 2919–32
- Soliman M A and Kaldas M M S 2019 Semi-active suspension systems from research to mass-market—a review *J. Low Freq. Noise Vib. Act. Control* **40** 1005–23
- T. M. T. S. Model 2012 Model 835 system for testing small dampers Manual' MTS Systems Corporation
- Vékás L 2008 Ferrofluids and magneto-rheological fluids *CIMTEC 2008—Proc. 3rd Int. Conf. Smart Mater. Struct. Syst.—Smart Mater. Micro/Nanosystems* **54**, 127–36
- Warke V, Kumar S, Bongale A and Kotecha K 2022 Design and evaluation of an MRF damper for semi-active vibration control of the machining processes *J. Instrum.* **17** 12017
- Zheng J, Li Z, Koo J and Wang J 2014 Magnetic circuit design and Multiphysics analysis of a novel MR damper for applications under high velocity *Adv. Mech. Eng.* **6**
- Zhu X, Jing X and Cheng L 2012 Magneto-rheological fluid dampers: a review on structure design and analysis *J. Intell. Mater. Syst. Struct.* **23** 839–73